Addendum II to ATBD

D. Le Vine, T. Meissner, F. Wentz and J. Piepmeier

This addendum documents change made to the ATBD between V1.3 and V2.0 of the algorithm which was implemented in February, 2013 and released to the public through the JPL PO.DAAC the week of February 18, 2013. V2.0 represents a compilation of all the changes that have been made since launch. The code was updated to include all the changes and then the entire data set was re-run. Some issues remain, such as the ascending/descending difference, but it is intended to keep the algorithm stable at V2.0 and hold-off on incremental changes until a major reprocessing is warranted.

I. Pointing Angle

Analysis of the radiometer and scatterometer response near coast lines and comparing ascending and descending looks, indicated an improvement could be made by adjusting the pointing of the Aquarius beams relative to the directions derived from the spacecraft nominal attitude. Considering the slightly different estimates resulting from the analyses of at RSS (Kyle Hilburn) and JPL (Alex Fore), a decision was made to keep the relative angles of the three beams the unchanged and to modify the pointing of Aquarius relative to the spacecraft the following:

Roll: - 0.51 degrees
Pitch: 0.16 degrees
Yaw: no change

These are angles of the Aquarius nadir vector relative to nominal nadir (perpendicular to the Earth surface). Positive pitch is “pitch up in the direction of motion of the spacecraft. Positive roll is right-hand rule with the thumb of the right hand in the direction of motion (X-axis) and the fingers in the direction of positive change.

The pre-launch and modified orientation of the beams is given in Table I. The angles are relative to the nominal coordinate system with X in the direction of motion, Y pointing toward the day-time side (i.e. Sun) and Z pointing toward the Earth surface (geodetic: pointing normal to the surface at the sub-satellite point). Yaw is zero in the table below.

Table 1: Beam pointing angles (spherical coordinates)

Beam	Measured Pre-Launch		Effective: V2.0*	
	Theta	Phi	Theta	Phi
Inner	25.8	9.8 (-80.2)	25.27	9.65 (-80.35)
Middle	33.8	-15.3 (-105.3)	33.35	-15.74 (-105.74)
Outer	40.3	6.5 (-83.5)	39.78	6.38 (-83.62)

*Spherical coordinates in the original (nominal) system. The effective Theta is the correct choice for determining the local angle of incidence at the ground.

A. Summary of changes:

Changing the pointing angle of the spacecraft necessitated changes in several of the tables used in the retrieval algorithm, partly because the local incidence angle was changed and partly because the location of the beam boresight on the surface changed. The changes made for V2.0 included the new GRASP-II antenna pattern (Section II below) and the high resolution land mask (Section V). The changes included:

a. Tables for land and sea-ice fraction
b. Tables for the land contamination (i.e. land in sidelobe) correction
c. Reflected galactic background
d. Radiometer APC (Antenna Pattern Correction: See below)
e. Regridding of data to account for pointing angle adjustment.

B. References for Pointing

Attachment A: Kyle Hilburn, Thomas Meissner and Frank Wentz, "Aquarius Pointing Analysis", Remote Sensing Systems report RSS-TR-021313, February 13, 2013.

Attachment B: Alex Fore, Simon Yueh and Adam Freedman, " Data-Driven Determination of Pointing Errors from Push-Broom type Remote Sensing Instruments".

II. Antenna Pattern:

The project has been provided with three models for the Aquarius radiometer antenna patterns:

a. Calculated patterns made at JPL using TICRA's GRASP software;
b. Patterns measured on a scale model of the Aquarius/SAC-D observatory;
c. Calculated patterns made at JPL using enhanced GRASP software that permitted including more elements of the structure (e.g. boom) and spacecraft.

The pre-launch algorithm and antenna pattern correction (APC) were based on the scale model patterns. But these were modified almost immediately after launch because the predicted cross polarization coupling did not yield good results. Tuning of the APC to agree with observations yielded results that seemed to be in better agreement with the theoretical (calculated) patterns.

Subsequently, new antenna patterns have been computed at JPL using an enhanced GRASP software and computers capable of including more of the spacecraft and antenna structure (e.g. the boom). It was decided to use these patterns in developing the APC and associated code for V2.0. The major difference between the APC in V2.0 and in V1.3 is an increase in spillover (off-earth fraction) by about 1.5%.

The pre-launch GRASP model used geometric optics (GO) and only considered the feed and the reflector without the spacecraft structures. In an effort to increase the fidelity of the model pattern a new pattern was generated in collaboration with the SMAP project. This new pattern, termed GRASP 2012, is a much higher fidelity pattern than the original 2005 model. The 2012 pattern used a Method of Moments (MoM) solution and included a full representation of the spacecraft based the Aquarius CAD model.

In the meantime, a test was conducted get insight into the off-Earth fraction ("spill-over") of the actual antennas. On January 10, 2013 a Cold Sky Maneuver was conducted over Brazil transitioning from a stable region of the Amazon to ocean to provide information about the backlobes. Analysis of this data is still underway, but a preliminary conclusion seems to support the conclusion that the increase in spillover was not justified and that the spillover in the APC used in V1.3 is more realistic. (For additional information, see Section 6.2.2 in AQ-014-PS-0015, "Aquarius Radiometer Post-Launch Calibration for Product Version 2" by J. Piepmeier, 19 February 2013.)

The APC is defined with respect to the Stokes vectors, I,Q and U.

A. APC Matrix for V1.3

Based on Scale Model patterns but with off-diagonal elements set to zero except for T3 where a term was needed in horns 1 and 2 to remove a bias in T3. The matrix below is A defined by TA = A^{-1} TB:

horn 1

1	1.0300	0.0000	0.0000
2	0.0000	1.0795	0.0000
3	-0.0032	0.0000	1.0433

horn 2

1	1.0338	0.0000	0.0000
2	0.0000	1.0977	0.0000
3	0.0000	0.0000	1.0658

horn 3

1	1.0420	0.0000	0.0000
2	0.0000	1.1175	0.0000
3	-0.0057	0.0000	1.0999

B. APC Matrix for V2.0

Used the "new" Grasp model patterns and a minimum least square fit to the simulator data. Then the off-diagonal elements for coupling to T3 to I and Q (i.e. column 3) and of I into T3 (row 3) were adjusted to be in good agreement with the polarization rotation observed during cold sky pitch maneuvers.

horn 1			
1	1.0448	-0.0383	0.0500
2	- 0.0030	1.0786	0.0300
3	-0.0009	-0.0258	1.0433

horn 2			
1	1.0497	-0.0343	0.0000
2	-0.0006	1.0593	0.0000
3	-0.0067	0.0111	1.0555

horn 3			
1	1.0580	-0.0344	0.0250
2	-0.0004	1.0485	0.0300
3	-0.0045	-0.0148	1.0489

III. Roughness Correction

A change was made to use the scatterometer σo_vv and NCEP wind fields to generate the roughness correction. This was an option being evaluated at V1.3 (see Section III of Addendum I). The following model is used in V2.0:

$$\Delta E_w = R'(W_{NCEP}, \sigma o'_{vv}) + A_0(W_{NCEP}) + [A_1(W_{NCEP}) \cos(\varphi_{rel}) + A_2(W_{NCEP}) \cos(2\varphi_{rel})] \quad \text{(III.1)}$$

where

ΔE_w = Change in emissivity due to roughness (III.2a)

W_{NCEP} = NCEP wind speed (III.2b)

φ_{rel} = Relative azimuth between beam boresight and wind direction (wind direction is determined using NCEP wind direction) (III.2c)

$\sigma o'_{vv} = \sigma o_{vv} - [B_1(W_{NCEP}) \cos(\varphi_{rel}) + B_2(W_{NCEP}) \cos(2\varphi_{rel})]$ (III.2d)

σo_{vv} = The observed scatterometer cross section at VV-polarization (III.2e)

$R'(W_{NCEP}, \sigma o'_{vv})$ = A two dimensional look-up table derived from the data and simulator (expected value of TA) (III.2f)

$R(W_{NCEP}, \sigma o'_{vv}) = R'(W_{NCEP}, \sigma o'_{vv}) + A_0(W_{NCEP})$ (III.2g)

= The "isotropic" portion of the emissivity correction (i.e. independent of wind direction)

A_0, A1, A_2, B_1, B_2 = Polynomials in wind speed. They are determined empirically; (III.2h)
The values sued in V2.0 are listed in Appendix A.

The procedure for determining the roughness correction, ΔE_w, is as follows. First the wind direction signal is removed from the observed scatterometer backscatter cross section, σo_{VV}, as shown in (III.2d). The wind field is obtained from NCEP and consists of wind speed, W_{NCEP} and direction relative to the antenna boresight, φ_{rel}. The coefficients A and B are determined empirically from Aquarius data by comparing observed and simulated data (see Appendix A). The corrected cross section, $\sigma o'_{vv}$, is used together with the NCEP wind speed, W_{NCEP} in the two dimensional look up table $R'(W_{NCEP}, \sigma o'_{vv})$ to get the direction-independent (i.e. isotropic) effect of roughness. The "table" is shown in Figure III.1.

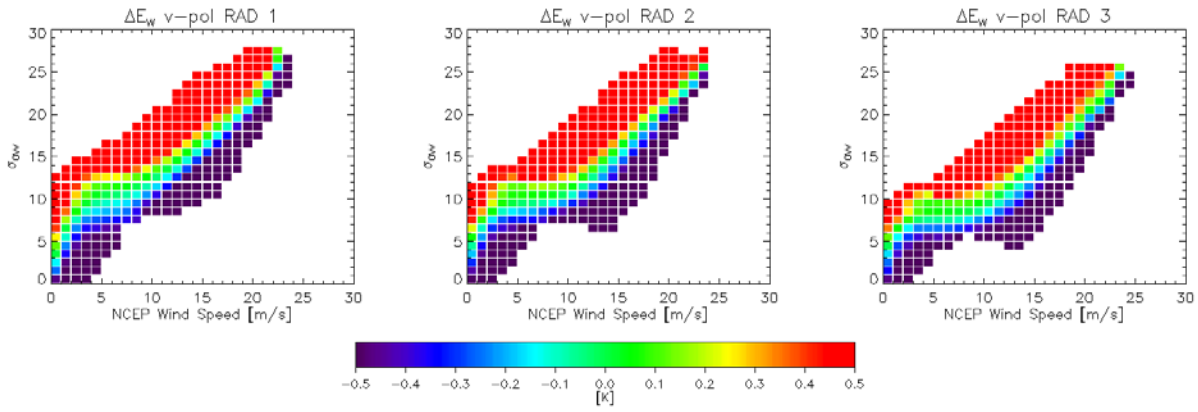

Figure III.1: The residual roughness correction map $R'(W_{NCEP}, \sigma o'_{vv})$

The $R'(W_{NCEP}, \sigma'_{0,VV})$ map is also associated with a histogram indicating the probability of occurrence of points in the 2-D map. If the value associated with W_{NCEP} and $\sigma_0'_{VV}$ falls outside bounds set for acceptable likelihood, then the A_0 coefficient in Equation III.1 which is a function of W_{NCEP} only is used instead of the lookup table in order to compute the isotropic part. The same is done if the value for $\sigma_{0,VV}$ is unavailable or flagged as RFI contaminated. In both cases a roughness correction flag is set. Finally, the wind direction dependent part (1st and 2nd harmonic contribution in equation III.1) is added to obtain the complete surface roughness signal. For its computation we use again NCEP wind speed and direction.

Comment: In Equation III.2d the parameter, σo_{vv}, is the measured (i.e. observed) value of the scatterometer cross section. This is in contrast to the value predicted from W_{NCEP} using the model function described in Appendix A part B.

IV. Drift Correction dTA

It was noticed soon after launch that the derived brightness temperatures were drifting compared to the reference ocean used for calibration. An example is shown in Figure IV.1. This is data for the outermost beam (radiometer 3) and vertical polarization. The drift is quite small, about 1 Kelvin in a year; however, the requirements for Aquarius are sufficiently stringent that a noticeable drift in retrieved SSS was observed. For additional information, see Sections 3 and 4 in AQ-014-PS-0015, "Aquarius Radiometer Post-Launch Calibration for Product Verstion 2" by J. Piepmeier, 19 February 2013.

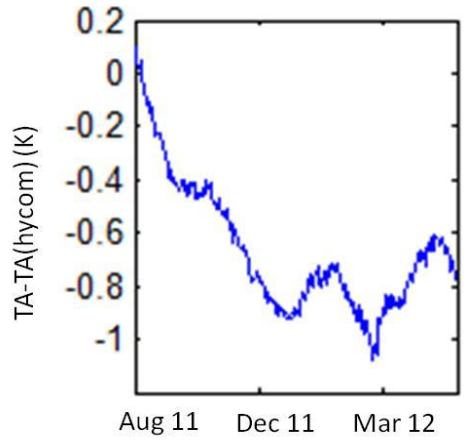

Fig IV.1: Difference between measured and predicted antenna temperature for radiometer 3 and vertical polarization.

The drift consists of two components, a monotonic exponential-like drift upon which are superimposed "wiggles" with an irregular period of several months. Evidence suggests that the drift is an instrument associated change in gain. The drift is corrected in V2.0 in two stages.

A. Exponential Drift Correction:

Motivated by reports of exponential changes in gain due to out-gassing, it was decided to fit an exponential change to each radiometer channel. This was done purely empirically, taking the entire radiometer history for each channel (V, p, m, H) and finding the best fit. Then the exponential, monotonic portion of the drift was subtracted from the history (e.g. Fig IV.1).

B. "Wiggles":

The remainder after removal of the exponential drift has an irregular, quasi-periodic behavior. Several hypotheses have been proposed to explain this behavior with no confirmation at this time. However, the consensus is that it is due to the instrument, and for V2.0 an approach based on this assumption has been implemented to remove the "wiggles"

The idea is to partition the data into several segments, for example Global (G), Ascending (A) and Descending (D), and then to compute the drift, dTA, for each segment by comparing with the expected TA for each:

$$dTA\big|_G = TA\big|_G - TA\_exp\big|_G \qquad \text{(IV.1)}$$

Average values are computed along an orbit for each partition (in this case, G, A, D) and then smoothed by taking the median value for one week (103 orbits). Now the difference between segments is computed:

$$DTA\big|_{G\text{-}A} = dTA\big|_G - dTA\big|_A \qquad \text{(IV.2)}$$

Assuming that the instrument errors are constant they will exist independent of the partition and cancel in the differences. The differences include only geophysical "error" which hopefully is small. The next step

is to find the coefficients of a linear regression of the double-differences in (IV.2) that best fits the single differences in (IV.1):

$$dTA\big|_G = R1\ DTA\big|_{G-A} + R2\ DTA\big|_{G-D} \quad \text{(IV.3)}$$

A minimum least square solution is sought over the entire data set (all orbits) using, for example a Moore-Penrose pseudo inverse. The "solution" is only a best fit because the DTA are orthogonal to the instrument error contained in the dTA. Solving for the R and letting:

$$dTF\big|_G = R1\ DTA\big|_{G-A} + R2\ DTA\big|_{G-D} \quad \text{(IV.4)}$$

Then an estimate of the instrument error, dTI, is obtained from the residual after solution:

$$dTI\big|_G = dTA\big|_G - dTF\big|_G \quad \text{(IV.5)}$$

The final result is averaged over the partitions.

The solution above (IV.5) will also include any signal that is common to the three partitions (G, A, D) and in the final step a second iteration is performed to try to remove this residual. The procedure above is repeated for two additional sets of partitions: a) Global (G), northern hemisphere (N) and southern hemisphere (S); and b) Global (G), northern hemisphere ascending (NA), northern hemisphere descending (ND), southern hemisphere ascending (SA) and southern hemisphere descending (SD). From the solution (IV.5) obtained with these three sets, a second iteration is performed to separate the minor differences. In this iteration, the three dTF obtained from each partition (Equation IV.4) replace the three partitions and the process is repeated. For examples and more details, see Sections 3 and 4 in AQ-014-PS-0015, "Aquarius Radiometer Post-Launch Calibration for Product Version 2" by J. Piepmeier, 19 February 2013.

C. Comments:

1. The instrumental drift determined above is treated as a gain drift. This was established by comparing the drift over different scenes (e.g. land and ocean). A gain drift should scale with the scene temperature and a bias should be independent of the scene. The change in gain indicated by the instrumental drift determined in (IV.5) is corrected by adjusting the temperature of the Aquarius reference noise diode. This temperature is changed enough to cause the required change in gain.

2. The exponential drift and the R-coefficients are updated once per week.

3. An hypothesis exists for the root cause of the "wiggles" and a plan exists to test this hypothesis on instrument hardware.

V. TB Consistency Parameter Added to the L2 Data:

A new metric has been added to the L2 data file that gives an indication of the consistency of the salinity retrieval. The metric is the mean square error between the measured brightness temperature and the predicted brightness temperature using horizontal polarization:

$$TB_{err} = \text{Sqrt}\ \{\ [TB_{H,meas} - TB_{H,model}(SSS_{Aq})]^2\ \} \quad \text{(V.1)}$$

where SSS_{Aq} is the retrieved value of salinity . This parameter is called "**rad_Tb_consistency**" in the L2 files.

The algorithm retrieves sea surface salinity, SSS_{Aq} using only radiometer measurements at vertical polarization. If the retrieval is good, then the retrieved value of salinity used in a forward model should predict values of brightness temperature at horizontal polarization (i.e. $TB_{H,model}(SSS_{Aq})$) reasonably close to those observed. Values of TB_{err} should be consistent with the performance of the algorithm. For example, if the global error compared to HYCOM is 0.5 psu, then TB_{err} should also be of the same order of magnitude. Values much different suggest a problem (e.g. in the instrument calibration of the H-pol or V-pol channel or in the retrieval).

VI. RFI algorithm tuning

The algorithm for detecting and mitigating (removing) RFI is described in Section 7 of AQ-014-PS-0015, "Aquarius Radiometer Post-Launch Calibration for Product Version 2" by J. Piepmeier, 19 February 2013. Two major changes have been made in V2.0:

a. Short accumulation 1 has been dropped from the data stream. This consists of the first two antenna measurements in each 120 ms sequence. They are averaged in hardware aboard the spacecraft and transmitted to the ground as one data sample. It was noticed that this sample was biased and particularly noisy. The noise biased the algorithm and increased in the false alarm rate. The cause has not been confirmed, but it seems to correlate with a switch. Dropping this measurement has only a small impact on the radiometer performance (NEDT) but made a significant improvement in the performance of the RFI detection/mitigation algorithm.

b. The detection thresholds were tuned using on-orbit parameters measured over ocean. The detection thresholds in the RFI algorithm are scaled by a parameter representing the NEDT of the radiometer. This value was set pre-launch based on laboratory measurements with the radiometers. The same values were used for each channel in the radiometer. However, data once in orbit indicated very different false alarm rates among channels of the same radiometer. A decision was made to choose parameters for each radiometer that gave consistent false alarm rates among the channels. The values were based on radiometer noise performance over open-ocean far from land. In V2.0 the radiometer channels are tuned to all have a false alarm rate of about 5% over open-ocean.

Work is underway to further optimize the algorithm. In particular, it is planned to employ separate thresholds for land and ocean. Also, a measure of the missed-detection rate is being sought. The goal is to have known values of false alarm and missed detection rates which can then be optimized to fit the measurement goal.

VII. Land Mask Changed to 1 km Resolution:

A problem with the retrieval algorithm in the vicinity of islands was tracked to poor resolution of the land-water boundary with the original 10 km resolution mask. Switching to the higher resolution 1 km mask correctly identified islands and improved the salinity retrieval. The 1 km Remote Sensing System mask is currently employed in V2.0.

The higher resolution and pointing adjustment (Section I) make a significant difference in the vicinity of small islands.

VIII. Issues remaining

The Aquarius salinity retrieval algorithm is working well and is approaching the goal of 0.2 psu (RMS globally each month). For details, see "Aquarius Salinity Validation Analysis", AQ-014-PS-0016, G. Lagerloef, 18 February 2013.

Several issues remain to improve the retrieval. These include:

A. Wind speed and surface roughness correction: V2.0 uses the NCEP wind speed for performing the surface roughness correction. Preliminary studies by RSS have shown that a significant improvement of the surface roughness correction algorithm can be achieved by using a wind speed that is retrieved using the scatterometer $\sigma 0_{HH}$ and radiometer TB_H. The impact of significant wave height for the surface roughness correction will also need to be analyzed.

B. Ascending/Descending difference: A bias exists between TB and retrieved SSS on ascending and descending passes over the same piece of ocean. Current thought is that this is geophysical in origin. That is, something in the correction the geophysical environment that is not properly compensated. One likely cause is an inaccurate correction for the galactic background radiation reflected from the ocean. It may be due to an error in the roughness model, including the model itself or the assumed ocean wave spectrum, for example. A correlation of the bias with the reflected galactic background has been demonstrated. Another potential cause is incorrect coupling, in the APC, of the third Stokes parameter into the first and second Stokes parameters (I and Q) which is related to the Faraday rotation correction. Undetected RFI has also been mentioned as a potential cause.

C. Undetected RFI: Persistent areas of ascending/descending bias and/or high RMS noise, for example, in the North Atlantic off the coast of Spain and France and in the Western Pacific off the coast of China, exist and undetected RFI has been mentioned as a potential cause (largely because there are areas of persistent RFI on land nearby).

D. Spillover and it impact on the APC and calibration: Any change in spillover will need to be combined with an adjustment of the noise diode temperature in order to preserve the calibration for ocean scenes. This will impact the calibration of Aquarius TB over land surfaces and also the cold space maneuver. Also, although the dynamic range of TB over the ocean is small, a change of the spillover factor by 1.5% can lead to a change in the observed crosstalk between SSS and SST.

E. Rain flag and/or correction: Currently, there is no flag for rain nor any attempt to correct the data when rain is present. A concern is that when a correction is attempted that it doesn't over correct and remove effects such as fresh water lenses. This is especially a worry for an algorithm that uses the HYCOM SSS as a reference which does not include such things (i.e. consequently, they could be removed as part of calibration). The use of the SAC-D MWR will aid in rain flagging and implementing a rain correction in the Aquarius radiometer observations.

F. The dielectric constant model: Research is needed to determine the differences between the models (e.g. Klein-Swift, Meissner-Wentz and George Washington University). The differences are particularly significant for cold water and very warm water.

G. Model for Atmospheric O2 emission: The model, which is based on the tails of resonant lines at higher frequencies, has never been fully verified by observations. One reason is that it is difficult to disentangle this effect from others such as the differences in the dielectric constant.

H. Land Correction: Retrieving SSS closer to land is needed to address areas such as the Gulf of Mexico and Mediterranean Sea and for applications in the ice melt areas of the North Atlantic.

IX. Appendix A: Coefficients for Roughness correction

A. Radiometer Wind Dependence:

The model function is:

$$\Delta E_w = A_0(W_{NCEP}) + [A_1(W_{NCEP}) \cos(\varphi_{rel}) + A_2(W_{NCEP}) \cos(2\varphi_{rel})]$$

The format for the coefficients, A, is: $A_I(W) = \sum a_N W^N$ where W = NCEP windspeed.

The tables below list the coefficients a_N for each A_I I = {0,1,2} and N = {1,2,3,4,5}. The first column is N, the second column is A0, the third column is A1 and the last column is A2.

N	A0	A1	A2

1. Beam 1 (inner) V-Pol

1	0.746918E+00	-0.117422E-01	0.228988E-01
2	-0.155767E+00	0.708212E-02	-0.113397E-01
3	0.162406E-01	-0.892835E-03	0.129482E-02
4	-0.716321E-03	0.466404E-04	-0.352189E-04
5	0.118677E-04	-0.800077E-06	-0.133351E-07

2. Beam 1 (inner) H-Pol

1	0.100418E+01	-0.191261E-01	-0.394986E-01
2	-0.200164E+00	0.477086E-02	0.208141E-01
3	0.203046E-01	-0.320980E-03	-0.327848E-02
4	-0.893943E-03	0.431747E-05	0.191358E-03
5	0.147887E-04	0.128809E-06	-0.384246E-05

3. Beam 2 (middle) V-pol

1	0.605605E+00	-0.175005E-01	0.333492E-01
2	-0.107905E+00	0.116026E-01	-0.146763E-01
3	0.101437E-01	-0.159345E-02	0.191895E-02
4	-0.393938E-03	0.900657E-04	-0.912087E-04
5	0.580947E-05	-0.172621E-05	0.154318E-05

4. Beam 2 (middle) H-pol

1	0.114136E+01	-0.304671E-01	-0.440811E-01
2	-0.213218E+00	0.118148E-01	0.196872E-01

```
 3   0.206956E-01  -0.139834E-02  -0.270319E-02
 4  -0.881868E-03   0.684264E-04   0.137093E-03
 5   0.141794E-04  -0.119226E-05  -0.238093E-05
```

5. Beam 3 (outer) V-pol

```
 1   0.569034E+00  -0.698267E-02   0.494216E-01
 2  -0.985977E-01   0.522038E-02  -0.172070E-01
 3   0.930263E-02  -0.609417E-03   0.170566E-02
 4  -0.372773E-03   0.335861E-04  -0.557595E-04
 5   0.581241E-05  -0.592229E-06   0.500398E-06
```

6. Beam 3 (outer) H-pol

```
 1   0.145126E+01  -0.137586E-01  -0.467308E-01
 2  -0.272426E+00   0.489583E-02   0.240198E-01
 3   0.266607E-01  -0.464281E-03  -0.362058E-02
 4  -0.117377E-02   0.174914E-04   0.205866E-03
 5   0.195821E-04  -0.188040E-06  -0.399987E-05
```

Note: The following extrapolation is made for high winds

A0: $W_{NCEP} > 28.5$: linear extrapolated

A1: $W_{NCEP} > 22.5$: kept constant above

A2: $W_{NCEP} > 22.5$: kept constant above

B. Scatterometer Wind Dependence

The model function is:

$$\sigma 0(W_{ncep}) = B_0(W_{NCEP}) + [B_1(W_{NCEP}) \cos(\varphi_{rel}) + B_2(W_{NCEP}) \cos(2\varphi_{rel})]$$

The format for the coefficients, B, is: $B_I(W) = \sum b_N W^N$ where W = NCEP windspeed.

The tables below list the coefficients b_N for each A_I I = {0,1,2} and N = {1,2,3,4,5}. The first column is N, the second column is B0, the third column is B1 and the last column is B2.

N	B0	B1	B2

1. Beam 1 (inner) VV-pol

```
 1   0.292127E-01   0.103254E-02   0.333935E-02
 2  -0.419578E-02  -0.402163E-03  -0.205659E-02
 3   0.324182E-03   0.514186E-04   0.296213E-03
 4  -0.108925E-04  -0.253892E-05  -0.143384E-04
 5   0.131611E-06   0.451332E-07   0.232583E-06
```

2. Beam 1 (inner) HH-pol

```
 1   0.132245E-01   0.738328E-03   0.212000E-02
 2  -0.136793E-02  -0.269368E-03  -0.117313E-02
 3   0.994375E-04   0.354814E-04   0.163053E-03
 4  -0.305969E-05  -0.164329E-05  -0.755614E-05
 5   0.318014E-07   0.275492E-07   0.117273E-06
```

3. Beam 2 (middle) VV-pol

```
 1   0.133574E-01   0.467148E-03   0.101017E-02
 2  -0.244474E-02  -0.180163E-03  -0.683601E-03
 3   0.211650E-03   0.242290E-04   0.103548E-03
 4  -0.777240E-05  -0.115860E-05  -0.501995E-05
 5   0.102361E-06   0.193816E-07   0.801823E-07
```

4. Beam 2 (middle) HH-pol

```
 1   0.390425E-02   0.222352E-03   0.458944E-03
 2  -0.603671E-03  -0.820249E-04  -0.274341E-03
 3   0.527038E-04   0.120613E-04   0.391840E-04
 4  -0.188745E-05  -0.509656E-06  -0.178050E-05
 5   0.237069E-07   0.715689E-08   0.266492E-07
```

5. Beam 3 (outer) VV-pol

```
 1   0.839614E-02   0.330010E-03   0.595045E-03
 2  -0.167107E-02  -0.128677E-03  -0.380667E-03
 3   0.151181E-03   0.168355E-04   0.600726E-04
 4  -0.572141E-05  -0.754948E-06  -0.300205E-05
 5   0.772311E-07   0.114974E-07   0.493874E-07
```

6. Beam (outer) HH-pol

```
 1   0.138710E-02   0.102528E-03   0.171524E-03
 2  -0.239447E-03  -0.384446E-04  -0.994456E-04
 3   0.219788E-04   0.570026E-05   0.147519E-04
 4  -0.797247E-06  -0.232269E-06  -0.698847E-06
 5   0.999050E-08   0.299299E-08   0.110438E-07
```

Note: The following extrapolation is made for high winds

B0: $W_{NCEP} > 25.5$: linear extrapolated

B1: $W_{NCEP} > 22.5$: kept constant above

B2: $W_{NCEP} > 22.5$: kept constant above